DOI: 10.31401/WS.2025.proc.03

Daily and Monthly Predictions of the Maximum CME Speed Index for Solar Cycle 25 Using Simplex Projection Method

Gerçeker K., Kilcik A.

Department of Space Sciences and Technologies, Akdeniz University Faculty of Science, 07058, Antalya, Türkiye
kemalhangerceker@gmail.com , alikilcik@akdeniz.edu.tr

Abstract

Coronal Mass Ejections (CMEs) and their speed are not only important indicators of solar activity, but also for geomagnetic activity. In this study, we present daily and monthly predictions for Solar Cycle 25 using the Maximum CME Speed Index (MCMESI) and the Simplex Projection method. By generating both short-term (daily) and long-term (monthly) predictions for MCMESI, we demonstrate the predictability of this parameter. The monthly mean data set was derived from daily values, and predictions for the continuation of Solar Cycle 25 produced using monthly mean MCMESI. Both datasets cover the period from May 1999 to January 2025. Predictions generated from the monthly mean data suggest that Solar Cycle 25 is expected to complete in the mid-2030s. Solar Cycle 25 appears to be stronger than Solar Cycle 24 in terms of amplitude. For the daily predictions, we successfully postcasted (re-predicted) the last week of December 2024 and the first week of January 2025 on a daily basis.

Keywords: Coronal Mass Ejection; Linear Speed; Nonlinear Prediction

1. Introduction

Solar activity drives space weather, which can disturb satellites, radio links, navigation, and even power grids. Coronal mass ejections (CMEs) play an important role in space weather; the fast CMEs and the southward interplanetary magnetic field are closely linked to powerful geomagnetic storms (Gonzalez et al., 1999; Nitta & Mulligan 2021).

The Maximum CME Speed Index (MCMESI) is the speed of the fastest CME in a given day. Studies show that MCMESI tracks solar and geospace conditions and is related to geomagnetic indices such as Ap and Dst (Kilcik et al., 2011; Kilcik et al., 2020). Therefore, prediction of the MCMESI leads to geomagnetic activity prediction and helps protect against the effects of geomagnetic storms. For the prediction, we used Empirical Dynamic Modeling (EDM) and its Simplex Projection method, which learns system behavior directly from data using time-delay embeddings and nearest-neighbor projections, without assuming fixed equations. These types of methods have repeatedly shown strong short-term predictive skills in complex, partially chaotic systems (Sugihara & May 1990; Sugihara et al., 2012; Ye et al., 2015).

Recent daily/near-daily prediction efforts in space weather focus mainly on geomagnetic indices driven by upstream solar-wind/IMF data, with machine learning and nonlinear models achieving multi-hour to day-ahead skill (e.g., Dst and Kp). Examples include LSTM/GP hybrids for multi-hour Dst, recurrent models for day-ahead Kp from solar wind inputs, operational Dst models, and image-aided day-ahead Dst predictions (Gruet et al., 2018; Wang et al., 2023). However, daily predictions built directly on CME-based indices such as MCMESI remain rare, leaving an opportunity for targeted nonlinear modeling.

In this study, the MCMESI is evaluated as a predictive driver and Simplex Projection is applied to produce monthly and daily predictions for Solar Cycle 25. Short-horizon behavior (e.g., 3–4 days), where nonlinear methods typically perform best, is also bench-marked using

CME information compiled by the SOHO/LASCO CDAW catalog (Yashiro et al., 2004; Gopalswamy et al., 2009).

2. Data and Methods

The CME data were taken from the SOHO/LASCO CDAW CME Catalog (https://cdaw.gsfc.nasa.gov/CME_list/). Then we selected the fastest CME for each day. The monthly mean MCMESI was obtained as the arithmetic mean of the daily speed of this CME for the time period of May 1999–January 2025. The temporal variations of the daily and monthly MCMESI data sets are presented in Figure 1.

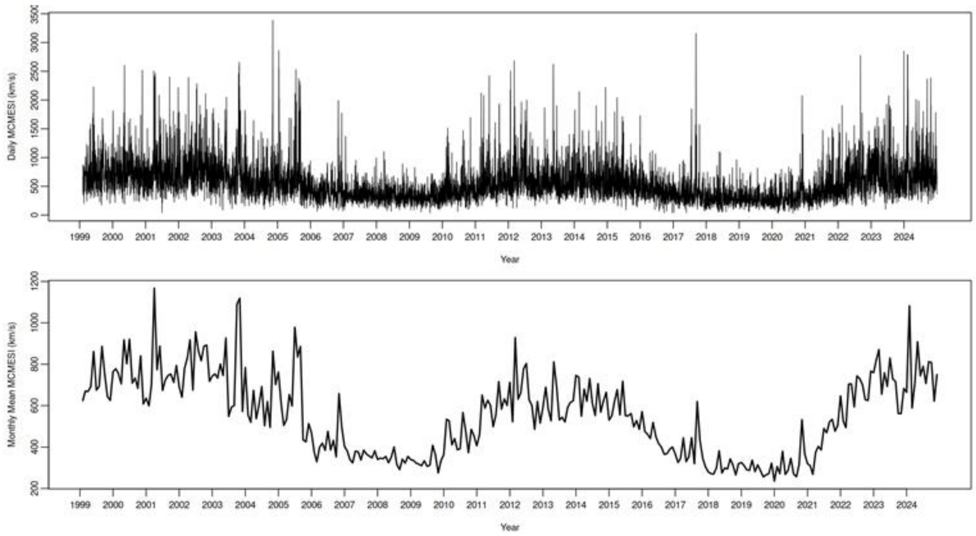

Figure 1. *Daily (top panel) and monthly mean (bottom panel) variations of the Maximum CME Speed Index (MCMESI).*

Following Takens' theorem (Takens 1981), the delay embedding

$$X(t) = [x(t), x(t-\tau), \dots, x(t-(E-1)\tau)], \quad (1)$$

was formed, where $X(t)$ is the state vector, $x(t)$ the scalar observation, τ the time delay, and E the embedding dimension. Proper choices of E and τ allow the reconstructed attractor to preserve the relevant geometry of the original system and thus support prediction.

For a current state vector $X(t)$, the $E+1$ nearest neighbors $X_1, X_2, \dots, X_{E+1}$ are identified. Let ν_n denote the current state and ν_i a neighbor with Euclidean distance $\|\nu_n - \nu_i\|$. Using the provided notation, the predictions for horizons $1,2,\dots,T_a$ are computed as

$$Pred_{[1,2,\dots,T_a]} = \sum_{i=1}^{E+1} \omega_i \, \nu^1_{(i+[1,2,\dots,T_a])}, \quad (2)$$

with exponential distance weights

$$\omega_i = \frac{exp\left(-\|\nu_n - \nu_i\|/\omega_{avg}\right)}{\sum_{j=1}^{E+1} exp\left(-\|\nu_n - \nu_j\|/\omega_{avg}\right)}, \quad (3)$$

where ω_{avg} is the average scaling factor. Multi-step predictions are obtained by iterating $Pred_{[1,2,\dots,T_a]}$. This equation-free, state-dependent procedure is standard in EDM and is well supported in nonlinear prediction (Sugihara 1990; Sugihara 2012; Ye 2015).

For the monthly data, the last 12 months were excluded from the data, and the first 12 predicted points were compared with the known excluded observations. For the daily series, the last 9 days data were excluded; the first 2 of these were used only for model selection, while the remaining 7 days were kept strictly unobserved and predicted forward. The selection was based on two complementary skill criteria; the Mean Absolute Error (MAE),

$$MAE = \frac{1}{N}\sum_{i=1}^{N}|x_i - \bar{x}|, \tag{4}$$

measure the average amplitude error in km/s and the Pearson correlation coefficient ρ,

$$\rho = \frac{\sum_{i=1}^{N}(x_i - \bar{x})(y_i - \bar{y})}{\sqrt{\sum_{i=1}^{N}(x_i - \bar{x})^2}\sqrt{\sum_{i=1}^{N}(y_i - \bar{y})^2}}, \tag{5}$$

Short-term behavior is emphasized on 3–4 day predictions. This is consistent with the general expectation that predictive ability in chaotic systems decreases with predefined time.

Possible values for E and τ were specified in advance ($E = 2 - 10, \tau = 1 - 30$). The split points defining the end of the library set and the beginning of the prediction set were sequentially scanned across a large portion of the data set, and all (E, τ) combinations were tested at each split point. Predictions for each scenario were generated based on ρ and MAE calculations. The best configurations were taken to be those yielding the highest ρ and lowest MAE values. The selected combinations were then used to generate the final predictions.

Simplex Projection method reconstructs the state space from a single time series and predicts by using the nearest past states and a distance-weighted average of their futures; no fixed equations are assumed, and only the embedding dimension E, time delay τ, and split point must be set. This equation-free, geometry-based design makes the approach data-efficient, easy to update as new values arrive, and appropriate when records are limited. In practice, short horizons are favored: daily predictions performed best for about 3–4 days, while longer (e.g., 7-day) horizons can still be produced with the expected loss of skill. These properties make Simplex Projection a natural choice for MCMESI and for other solar/geomagnetic indices that exhibit state-dependent behavior.

3. Results

The monthly MCMESI series was produced by averaging the daily MCMESI from May 1999 to January 2025. To test true out-of-sample skill, the last 12 months data (January–December 2024) were excluded from the data as a validation block. For Simplex Projection parameter combinations, candidate (E, τ) and split point values were predetermined within a certain range; a continuation model was created for each candidate starting from January 2024. The first 12 predicted points were then compared with the held-out observations using ρ and MAE, and the settings giving highest ρ and lowest MAE were retained. The selected configuration was finally used to produce the monthly cycle continuation presented in Figure 2.

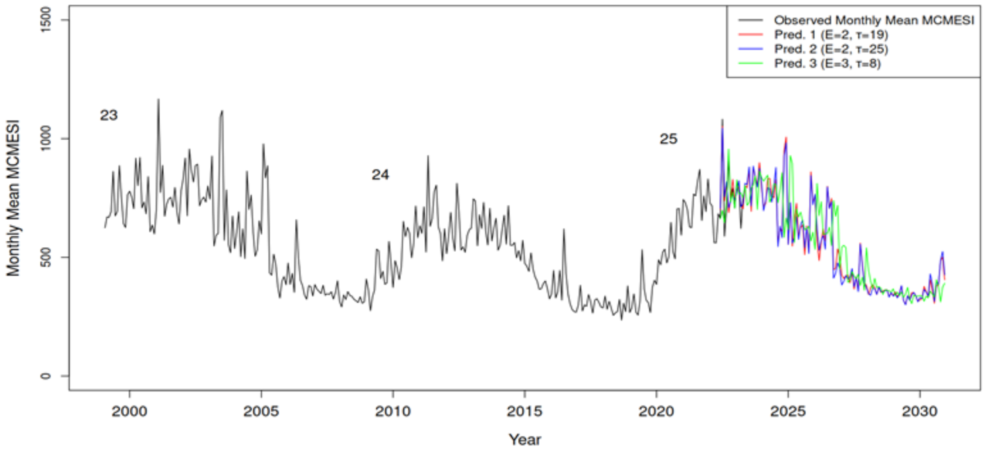

Figure 2. *Predictions for the continuation of Solar Cycle 25 produced using monthly mean MCMESI.*

A total of 90 monthly predictions were generated for the monthly data (12 held-out months of 2024 plus a 78-month period). The best-performing settings were determined by comparing the first 12 prediction points with the 12 held-out observations using MAE and ρ; the configuration with the highest ρ and lowest MAE value was ranked highest. The three best-performing configurations were retained, and their cycle continuations are shown in Figure 2. These continuations indicate that Solar Cycle 25 is stronger than Solar Cycle 24 in terms of the amplitude of the MCMESI, but slightly weaker or similar to Solar Cycle 23. The trajectories show a steady decline after 2025, with the cycle completing in the early to mid-2030s. High activity is also projected between 2024 and 2027, indicating the period of most intense geoeffective conditions in this cycle.

The daily MCMESI series was analyzed with the same Simplex Projection framework. To evaluate true short-horizon skill, 9 end-of-record values were withheld (the last week of 2024: 2 points used only for model selection and 7 points kept strictly unseen for prediction). Candidate (E, τ) and split point sets were pre-specified; three best combinations were retained based on the highest ρ and lowest MAE, and used to generate the 7-day forward predictions as shown in Figure 3.

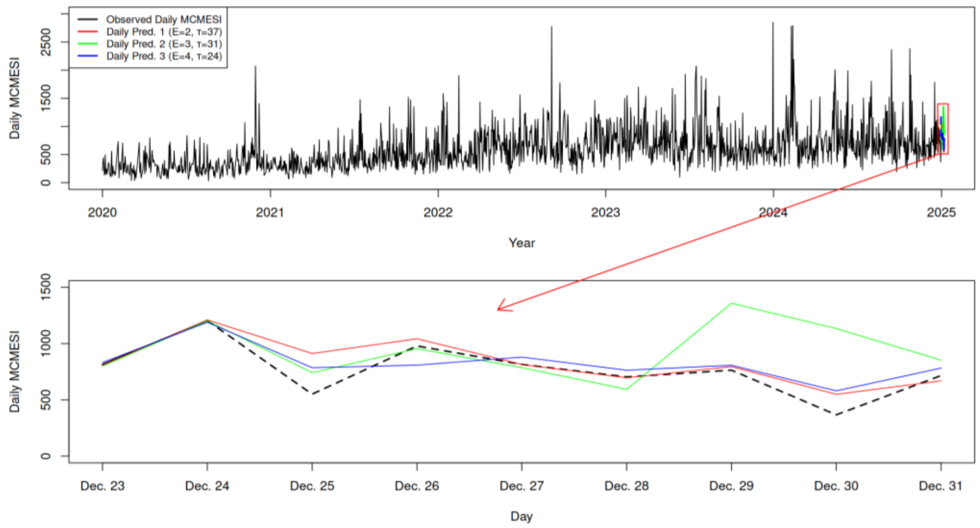

Figure 3. *Predictions for the last 9 days (2 observed + 7 considered unobserved) of 2024 generated using daily MCMESI values.*

As a first step, the three most successful predictions selected are closely aligned with the 2 observed points, indicating that the current situation is well captured. Over the next 7 days, the predicted trajectories reproduce the week's development in both shape and amplitude quite well, indicating good short-term prediction performance for the daily MCMESI.

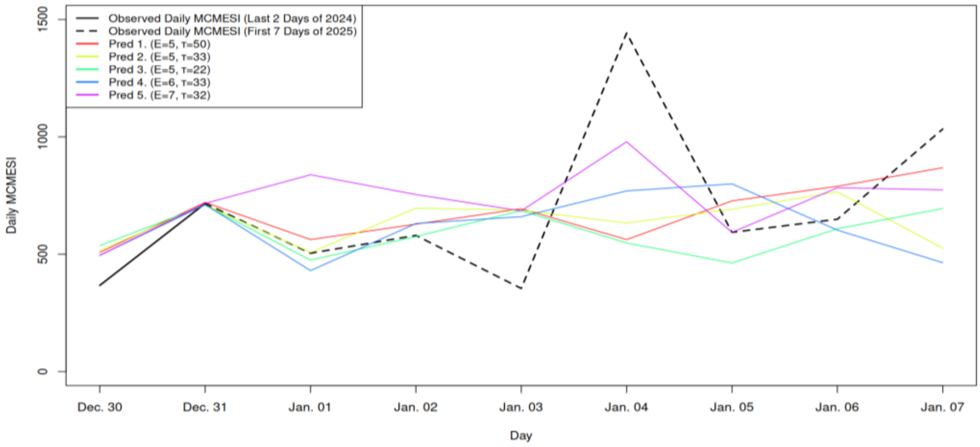

Figure 4. *Daily MCMESI predictions across the 2024→2025 boundary using a 2+7 setup. Predictions were initialized with the last 2 observed days of 2024 (Dec 30–31) and extended over 7 unobserved days (Jan 1–7, 2025); the subsequently published Jan 1–7 observations are overplotted as a dashed black line for validation.*

As shown in Figure 4, 9 days were analyzed using the 2+7 design as we entered 2025: the last 2 days of 2024 were used for parameter selection, and the following 7 days were predicted. Five predictions from the retained (E, τ) combinations are displayed in the figure. The most successful settings involved higher embedding dimensions E than in the previous week, suggesting a more complex state-space in the first week of 2025. The predictions and observations made during the first three days (January 1-3) showed good agreement, but in subsequent stages, performance declined as expected with increasing time. If the prediction had been initialized on Jan 3 (i.e., using three observed points for selection), the Jan 4 peak would likely have been captured more accurately. Overall, week-long predictions are feasible, but for precision and operational use, 3–4 day horizons are generally preferable.

From the monthly predictions, Solar Cycle 25 was predicted to exceed Cycle 24 in maximum CME-speed amplitude and to be slightly weaker or comparable to Cycle 23; activity was projected to decline after ~2025, with cycle completion in the early–mid 2030s. The 2024–2027 interval was identified as the most active part of the cycle, implying the highest geoeffectivity. In the daily analysis, the 2+7 design produced close agreement for the first 3–4 days, while skill decreased at longer times; in some weeks, higher embedding dimensions (E) were selected, indicating temporally varying complexity in the dynamics. Overall, Simplex Projection was applicable and efficient method for MCMESI prediction. While 3–4-day time intervals are recommended for predictions, a one-week prediction can be published with appropriate precautions.

4. Conclusion and Discussion

In this study, MCMESI-based predictions were performed on a monthly and daily basis using the Simplex Projection method. The findings of the study are as follows:

1. Solar Cycle 25 is stronger than Solar Cycle 24 in MCMESI amplitude and slightly weaker or comparable to Solar Cycle 23.

2. 2024–2027 is indicated as the most geo-effective interval of Solar Cycle 25. MCMESI activity declines after ~2025; cycle completion is predicted for early–mid 2030s.
3. For daily predictions, best agreement occurs over ~3–4 days; week-long predictions are feasible but show the expected loss of skill with time.
4. It has been proven that the Simplex Projection method can be applied to monthly and especially daily MCMESI data.

Based on monthly data, our MCMESI predictions indicate that Solar Cycle 25 (SC25) has exceeded SC24 and is slightly weaker than or comparable to SC23, with activity declining after ~2025 and reaching a minimum in the early to mid-2030s. This picture is broadly consistent with prediction-oriented cycle studies that anticipated SC25 to be similar to or somewhat stronger than SC24 and peaking near 2024 (e.g., Bhowmik & Nandy 2018), while remaining well below the most optimistic "very strong SC25" scenarios inferred from terminator-based arguments (McIntosh et al., 2020). It also sits between competing physics-based predictions that predicted either a weaker-than-SC24 (Upton & Hathaway 2018) or a substantially stronger one (McIntosh et al., 2020), and is consistent with review assessments of SC25 predictions that emphasized the spread across methods (Petrovay 2020).

On a daily basis, the 2+7-day design provided the highest compatibility for ~3–4 days, followed by the expected skill loss over longer periods. This short-horizon character aligns with operational geomagnetic-index prediction results: data-driven/ML and hybrid models for Dst and Kp typically achieve multi-hour to day-ahead skill but degrade with time (e.g., Temerin & Li 2006; Gruet et al., 2018; Hu et al., 2023). Our CME-based prediction tool, which relies on a single series, provides useful predictions for 3–4 days without upstream solar wind inputs, but shares the same fundamental limitation of decreasing accuracy over time.

Relative to event-level CME arrival time prediction, our approach plays a complementary role. Physics-based and drag-based systems (e.g., WSA–ENLIL+Cone, DBM/DBEM) generally report typical absolute arrival-time errors of order 10–15 hours and are strongest when detailed CME parameters are available; ensemble variants quantify uncertainty. In contrast, MCMESI-Simplex, rather than predicting the arrival time of individual CMEs, provides continuous predictions at the index level regarding amplitude and short-term evolution, indicating periods of high activity. Combining event timing models for specific CME events with MCMESI's index-level predictions can provide perspectives on both when and how they will be active (e.g., Mays et al., 2015; Napoletano et al., 2022).

Finally, higher embedding dimensions likely reflect temporally varying state complexity. This behavior has also been observed in studies where model skill depends on prevailing solar-wind/CME conditions.

Acknowledgements

This study was supported by Project 124N011 awarded by the Scientific and Technological Research Council of Türkiye (TÜBİTAK). We would also like to thank the Bulgarian Academy of Sciences (BAS) for their partial support.

References

Bhowmik, P., Nandy, D. (2018). Prediction of the strength and timing of sunspot cycle 25 reveal decadal-scale space environmental conditions, *Nature Communications*, Vol. 9, 5209, DOI: 10.1038/s41467-018-07690-0.

Gonzalez, W.D., Tsurutani, B.T., Clúa de Gonzalez, A.L. (1999). Interplanetary origin of geomagnetic storms, *Space Science Reviews*, Vol. 88, No. 3, pp. 529–562, DOI: 10.1023/A:1005160129098.

Gopalswamy, N., Yashiro, S., Michalek, G., Stenborg, G., Vourlidas, A., Freeland, S., Howard, R. (2009). The SOHO/LASCO CME catalog, *Earth, Moon, and Planets*, Vol. 104, No. 1, pp. 295–313, DOI: 10.1007/s11038-008-9282-7.

Gruet, M.A., Chandorkar, M., Sicard, A., Camporeale, E. (2018). Multiple-hour-ahead forecast of the Dst index using a combination of long short-term memory neural network and Gaussian process, *Space Weather*, Vol. 16, No. 11, pp. 1882–1896, DOI: 10.1029/2018SW001898.

Hu, A., Camporeale, E., Swiger, B. (2023). Multi-hour-ahead Dst index prediction using multi-fidelity boosted neural networks, *Space Weather*, Vol. 21, No. 4, e2022SW003286, DOI: 10.1029/2022SW003286.

Kilcik, A., Chowdhury, P., Sarp, V., Yurchyshyn, V., Donmez, B., Rozelot, J.P., Ozguc, A. (2020). Temporal and periodic variation of the MCMESI for the last two solar cycles; comparison with the number of different class X-ray solar flares, *Solar Physics*, Vol. 295, No. 11, 159, DOI: 10.1007/s11207-020-01711-2.

Kilcik, A., Yurchyshyn, V.B., Abramenko, V., Goode, P.R., Ozguc, A., Rozelot, J.P., Cao, W. (2011). Time distributions of large and small sunspot groups over four solar cycles, *Astrophysical Journal*, Vol. 731, No. 1, 30, DOI: 10.1088/0004-637X/731/1/30.

Mays, M.L., Taktakishvili, A., Pulkkinen, A., MacNeice, P.J., Rastätter, L., Odstrčil, D., Kuznetsova, M.M. (2015). Ensemble modeling of CMEs using the WSA–ENLIL+ Cone model, *Solar Physics*, Vol. 290, No. 6, pp. 1775–1814, DOI: 10.1007/s11207-015-0692-1.

McIntosh, S.W., Chapman, S., Leamon, R.J., Egeland, R., Watkins, N.W. (2020). Overlapping magnetic activity cycles and the sunspot number: Forecasting sunspot cycle 25 amplitude, *Solar Physics*, Vol. 295, No. 12, 163, DOI: 10.1007/s11207-020-01723-y.

Napoletano, G., Foldes, R., Camporeale, E., de Gasperis, G., Giovannelli, L., Paouris, E., Del Moro, D. (2022). Parameter distributions for the drag-based modeling of CME propagation, *Space Weather*, Vol. 20, No. 9, e2021SW002925, DOI: 10.1029/2021SW002925.

Nitta, N.V., Mulligan, T., Kilpua, E.K., Lynch, B.J., Mierla, M., O'Kane, J., Zhukov, A.N. (2021). Understanding the origins of problem geomagnetic storms associated with "stealth" coronal mass ejections, *Space Science Reviews*, Vol. 217, No. 8, 82, DOI: 10.1007/s11214-021-00857-0.

Petrovay, K. (2020). Solar cycle prediction, *Living Reviews in Solar Physics*, Vol. 17, No. 1, 2, DOI: 10.1007/s41116-020-0022-z.

Sugihara, G., May, R., Ye, H., Hsieh, C.-H., Deyle, E., Fogarty, M., Munch, S. (2012). Detecting causality in complex ecosystems, *Science*, Vol. 338, No. 6106, pp. 496–500, DOI: 10.1126/science.1227079.

Sugihara, G., May, R.M. (1990). Nonlinear forecasting as a way of distinguishing chaos from measurement error in time series, *Nature*, Vol. 344, No. 6268, pp. 734–741, DOI: 10.1038/344734a0.

Takens, F. (1981). Detecting strange attractors in turbulence, in: Rand, D., Young, L.-S. (eds), *Dynamical Systems and Turbulence, Warwick 1980, Lecture Notes in Mathematics*, Vol. 898, Springer, Berlin, Heidelberg, DOI: 10.1007/BFb0091924.

Temerin, M., Li, X. (2006). Dst model for 1995–2002, *Journal of Geophysical Research: Space Physics*, Vol. 111, A4, DOI: 10.1029/2005JA011257.

Upton, L.A., Hathaway, D.H. (2018). An updated solar cycle 25 prediction with AFT: The modern minimum, *Geophysical Research Letters*, Vol. 45, No. 16, pp. 8091–8095, DOI: 10.1029/2018GL078387.

Wang, J., Luo, B., Liu, S., Shi, L. (2023). A machine learning-based model for the next 3-day geomagnetic index (Kp) forecast, *Frontiers in Astronomy and Space Sciences*, Vol. 10, 1082737, DOI: 10.3389/fspas.2023.1082737.

Yashiro, S., Gopalswamy, N., Michalek, G., St. Cyr, O.C., Plunkett, S.P., Rich, N.B., Howard, R.A. (2004). A catalog of white light coronal mass ejections observed by the SOHO spacecraft, *Journal of Geophysical Research: Space Physics*, Vol. 109, A7, DOI: 10.1029/2003JA010282.

Ye, H., Beamish, R.J., Glaser, S.M., Grant, S.C., Hsieh, C.-H., Richards, L.J., Sugihara, G. (2015). Equation-free mechanistic ecosystem forecasting using empirical dynamic modeling, *Proceedings of the National Academy of Sciences*, Vol. 112, No. 13, pp. E1569–E1576, DOI: 10.1073/pnas.1417063112.